POLITECNICO DI TORINO
Repository ISTITUZIONALE

Testing and integration of the S-Band chain on the Cubesat Control Centre

Original
Testing and integration of the S-Band chain on the Cubesat Control Centre / Di Pasquale, S., Storace, A., Corpino, S., Stesina, F., Borlina, E., Mazzuca, B., Di Nuzzo, A., Sanino, F., Abbate, G., Cazacu, D.A., Taretto, A., Campioli, S.. - (2026). (77th International Astronautical Congress, IAC 2026 Belek (Tur) 5-9 October 2026).

Availability:
This version is available at: 11583/3016677 since: 2026-10-15T09:41:51Z

Publisher:
International Astronautical Federation, IAF

Published
DOI:

Terms of use:

This article is made available under terms and conditions as specified in the corresponding bibliographic description in the repository

Publisher copyright

(Article begins on next page)

27 November 2026

Copyright ©2026 by the International Astronautical Federation (IAF). All rights reserved.

IAC-26,B2,IP,29,x116371

Testing and integration of the S-Band chain on the Cubesat Control Centre

Sara Di Pasquale [b]*, Aleksandr Storace [a] , Sabrina Corpino [a], Fabrizio Stesina [a], Edoardo Borlina [c], Bruno Mazzucca [c], Alessandro Di Nuzzo [a], Fabio Sanino[c], Giorgio Abbate [a], Daniel Alexandru Cazacu[b], Alessio Taretto [a], Serena Campioli [a]

[a] *Department of Mechanical and Aerospace Engineering, Politecnico di Torino, Italy* s309728@studenti.polito.it giorgio.abbate@studenti.polito.it , s353598@studenti.polito.it , alessio.taretto@studenti.polito.it , serena.campioli@polito.it , sabrina.corpino@polito.it , fabrizio.stesina@polito.it

[b] *Department of Electronics and Telecommunications, Politecnico di Torino, Italy* s323151@studenti.polito.it , danielalexandru.cazacu@studenti.polito.it

[c] *Department of Control and Computer Engineering, Politecnico di Torino, Italy* edoardo.borlina@gmail.com , s325664@studenti.polito.it , s326369@studenti.polito.it

* Corresponding Author

Abstract

With the constant demand for higher data rates to accommodate increasingly sophisticated and high-performance payloads on CubeSats, the need to migrate toward less congested frequency bands and wider bandwidth allocations are becoming increasingly evident. In this context, as the development of the ground infrastructure - the CubeSat Control Centre (C3) — approaches its final stages, the CubeSat PoliTO Team at Politecnico di Torino is focusing on the testing and finalization of the S-band communication chain, aimed at enabling enhanced downlink and uplink capabilities.
The team has been developing, operating, and maintaining C3 as both a ground station and a mission control center, with the educational objective of enabling students to manage end-to-end space missions. C3 currently supports communications in amateur VHF and UHF bands and is being extended to include S-band capabilities.
Following the successful testing and integration of the VHF and UHF RX and TX chains, the team has focused on the development, testing and validation of the S-band communication line. The campaign began with the characterization of individual RF components, including amplifiers stages and cables. Key parameters such as S-parameters, gain, matching, and spectral performance were measured using a Vector Network Analyzer (VNA) and Spectrum Analyzers (SA). A progressive integration approach was adopted, incrementally combining validated components until the complete RX and TX chains were assembled and verified also to maximize the educational output value. Although the selected RF amplifiers are commercial off-the-shelf (COTS) units, the integration within the existing ground station architecture required the development of dedicated custom support boards. These boards provide proper biasing, protection circuitry, and electrical interfacing, ensuring seamless integration with the broader C3 system.
Beyond the technical achievements, the project carries a strong formative impact. The S-band upgrade provided team members, coming from diverse academic backgrounds, with hands-on experience in RF design, measurement techniques, system engineering, and structured AIV-T processes. The activity fostered interdisciplinary collaboration, practical problem-solving skills, and a deeper understanding of real-world ground segment development.
This paper presents the design choices underlying the S-band communication chain, the integration challenges encountered when interfacing with a pre-existing multi-band ground station, and the development of custom hardware solutions to bridge gaps between COTS components and the rest of the system. The adopted testing philosophy, based on incremental validation and educational return, is discussed providing reference practices for similar academic ground stations.

Keywords: CubeSat, Ground Station, Satellite Control Center, Radio Frequency, S-band

Copyright ©2026 by the International Astronautical Federation (IAF). All rights reserved.

Nomenclature
TX: Transmission
RX: Reception
TRX: Transmission and Reception

Acronyms/Abbreviations

C3: CubeSats Control Centre
GS: Ground Station
LEO: Low Earth Orbit
TLE: Two-Line Elements
UHF: Ultra High Frequency
VHF: Very High Frequency
RF: Radio Frequency
COTS: Components Off The Shelf
AIVT: Assembly Integration Verification Testing
FSPL: Free Space Path Loss
SDR: Software Defined Radio
FPGA: Field Programmable Gate Arrays
BPSK: Binary Phase-Shift Keying
GUI: Graphical User Interface
HPA: High Power Amplifier
LNA: Low Noise Amplifier
NF: Noise Factor
DUT: Device Under Test
RBW: Resolution Bandwidth
VNA: Vector Network Analyzer
SA: Spectrum Analyzer
RFI: Radio Frequency Interference
EMI: ElectroMagnetic Interference

1. Introduction to C3

1.1 What is C3

The Cubesat Control Centre (C3) of the Polito CubeSat Team [1] is a student operated ground station finalized to the learning and the studying of the dynamics behind space satellite communications. The project was born with the intention of fulfilling the desire to organize and design a satellite mission both for the space segment and the ground segment. Before the birth of C3 the Team relied for the previous missions on Radio-Amateurs GS, but for future missions, the desire is to handle the communications in house. C3 currently has fully tested and operational UHF and VHF communication chains [2,3].
The project encompasses the installation of antennas on the roof of Politecnico di Torino, though the physical deployment is currently delayed due to administrative hurdles. Once the parabolic antenna is ready and in position, communications will be ensured by distance with the use of a private site that tracks (thanks to a TLE reading code that permits to rotate the rotor in the desired trajectory) and transmits/receives data from the selected satellite.

1.2 The needing of the S-band

As previously mentioned, the C3 ground station was built to support the team's upcoming satellite missions [1], which is exactly why the team decided to integrate an S-band module. Increasing CubeSat data volumes, together with bandwidth restrictions and spectrum congestion, create challenges for payload-data downlink [2,3]. For C3, the S-band upgrade is intended to support the higher data rates required by upcoming missions. A link that could guarantee reliable uplink and downlink communications with satellites in LEO was fundamental. This is especially critical for the downlink, where payload data volumes are much larger. Given the short visibility windows during a LEO pass over C3, achieving a higher data rate is essential to download everything in time. Implementing the S-band ensures the bandwidth necessary to handle these heavy data transfers and successfully close the high-speed link budget.
More about the next mission can be found in [2,3,4] and in Chapter 7.

2. S-band pipeline and main components

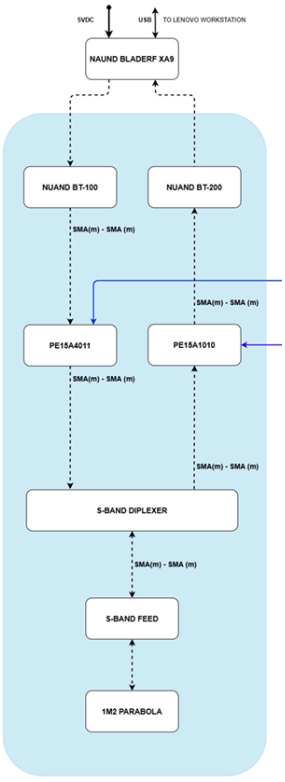

Fig. 1. S-Band RF Front-End

Copyright ©2026 by the International Astronautical Federation (IAF). All rights reserved.

Fig. 1 illustrates the overall S-band RF front-end pipeline alongside the key components detailed in the following subsections. The modules are interconnected using LMR-200 coaxial cables and standard SMA connectors; the insertion losses introduced by these short interconnections were considered negligible for the scope of the bench testing campaign. To manage power distribution safely, each amplifier is paired with a dedicated power MOSFET to switch and regulate current flow. These switches are controlled via GPIO by a centralized Raspberry Pi 4, which also manages power cycling for the rest of the ground station's subsystems. For the RF radiation segment, a 1.2-meter parabolic dish is utilized to provide the directivity and link gain strictly required for LEO S-band tracking, although it was not directly characterized during this bench campaign. All active stages are powered from a central 12 V DC supply, with the High-Power Amplifier (HPA) requiring a dedicated power splitter, as detailed in Section 2.3.1.

2.1 PASTERNACK PE15A1010

In any satellite downlink, the signal arriving at the ground station is incredibly weak due to Free Space Path Loss (FSPL). The primary Low Noise Amplifier (LNA) integrated is the PE15A1010 [6]. According to Friis' formula [5], the noise figure of this first amplifier dominates the entire receiving chain [6], meaning it must amplify the faint telemetry without adding thermal noise. This model was selected because it boasts an ultra-low Noise Figure of just 0.9 dB (1.1 dB max) and delivers a massive 40 dB of gain across the 2 GHz to 6 GHz range. This easily overcomes subsequent insertion losses from the coaxial cables. Furthermore, it maintains high linearity, preventing strong adjacent terrestrial signals from saturating the receiver.

2.2 NUAND BT-200

Despite the primary LNA being a crucial component for the RX pipeline, the signal still suffers attenuation as it travels down the feedline to the control room. The BT-200 serves as a secondary gain stage directly at the SDR input, effectively lowering the noise figure of the SDR itself and maximizing the receiver's dynamic range just before analog-to-digital conversion [7]. Designed specifically for SDRs, this module is powered entirely over the SMA connector via a bias-tee, eliminating the need for a separate DC power supply on the desk. It adds +16 dB of gain at 2.4 GHz while keeping the noise figure under 1.8 dB. One major advantage of this setup is its ability to dynamically bypass or enable the BT-200 directly through GNU Radio, allowing on-the-fly gain staging if a satellite pass is exceptionally strong [7].

2.3 PASTERNACK PE15A4011

Uplinking commands to a LEO satellite in the S-band requires immense power, as atmospheric attenuation and FSPL are significantly harsher at 2.4 GHz than on UHF/VHF bands. Because the SDR alone cannot output enough RF power to close the uplink budget, the PE15A4011 serves as the final, high-power stage of the transmission line. This GaAs Amplifier was chosen for its solid-state power amplifier that pushes up to 5 W of RF power, which is critical for punching through atmospheric losses. It provides a typical gain of 32 dB in the 2 GHz to 4.4 GHz range [8], perfectly matching the S-band target.

2.3.1 Power splitter design

The primary challenge in integrating the High-Power Amplifier was managing its strict DC biasing requirements. The HPA requires both a negative gate voltage (Vgs = -1 V) and a positive drain voltage (Vds = 8 V) [8]. Crucially, to prevent catastrophic damage to the amplifier's internal circuitry, the 8 V drain voltage must strictly be applied after the negative gate bias is fully established. To handle this mandatory power sequencing and support the component's high current draw using only a central 12 V DC supply, this custom power distribution and sequencing circuit was designed and is shown in Fig. 2.

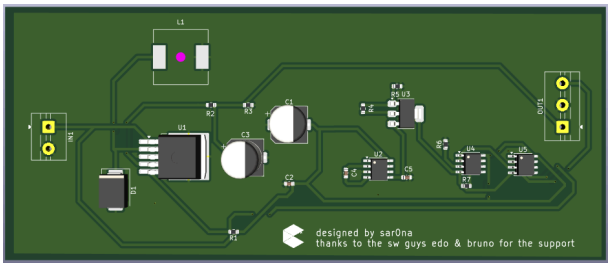

Fig. 2. Power Splitter PCB

2.4 NUAND BT-100

A high-power amplifier like the PE15A4011 requires a strong input signal to reach its maximum 5W output [8], but most SDRs output a very weak TX signal (often around 0 dBm or less). The BT-100 acts as the crucial driver stage, taking the low-power TX signal from the SDR and boosting it to the level required to properly drive the main PA. Like its RX counterpart, it draws power directly from the SDR's SMA connector via bias-tee, significantly simplifying the TX wiring diagram. It delivers approximately +11 dB of gain at 2.4 GHz [9]. Crucially, it ensures that the modulated S-band signals remain perfectly linear and undistorted before hitting the final PA, which is essential for preventing bit errors at the satellite's receiver.

Copyright ©2026 by the International Astronautical Federation (IAF). All rights reserved.

2.5 JFCD1400T2400SF Diplexer

Because the ground station shares a single parabolic dish for both transmitting and receiving, the JQL JFCD1400T2400SF cavity diplexer acts as the critical traffic controller at the antenna feed. Without it, the transmission from the HPA would leak directly into the RX line and instantly destroy the sensitive primary LNA.This SATCOM diplexer was selected because it safely handles up to 200 Watts of RF power [10] while providing a massive 50 dB of isolation between paths [10], perfectly protecting the receiving electronics during active transmission. Crucially for the link budget, its cavity-filter design introduces an incredibly low insertion loss of just 0.4 dB [10], ensuring the weak satellite downlink is not attenuated before reaching the LNA. Its hardware band splits also perfectly match the requirements [14], cleanly dividing the typical S-band uplink (2.025–2.120 GHz) from the downlink (2.200–2.400 GHz).

3. Organization of the test campaign

The test campaign for the C3 ground station was structured around a *Divide et Impera* (divide and conquer) approach, strictly following Assembly, Integration, Verification, and Testing (AIVT) cornerstones. To maintain a safe and organized workflow, verification methods aligned with the ECSS standards approved by ESA [11].

3.1 Hardware and Instrumentation

To reduce system complexity, C3 is primarily built using Commercial Off-The-Shelf (COTS) components, paired with open-source software like GNU Radio [12] to ensure compatibility with external research groups. Given budget constraints and the educational nature of the project, most of the RF testing was conducted using portable amateur instrumentation, such as Nano-VNAs, Nano-SAs, and calibrated bidirectional couplers.

This approach allowed the team to experiment, learn, and make mistakes, like driving amplifiers into saturation, without the fear of damaging expensive laboratory equipment. While amateur tools can sometimes yield noisy readings due to instrument sensitivity (such as the noise factor estimation in Chapter 5.1.2), all the devices used were calibrated according to professional lab equipment requirements [11,13]. This ensured the readings to be accurate enough to verify C3's requirements and identify component anomalies [2,3,14]. Furthermore, working with high-power RF sources introduces personnel safety risks and risks to electronics; to mitigate this, RF attenuators and dummy loads were utilised to control RF emissions and stay within the instrumentation's limits.

3.2 The testing pipeline

To keep the AIVT plan straightforward, the communication system was splitted into transmission and receiving lines and followed an incremental testing loop. The evaluation campaign began with the individual components in unit tests, using a Nano-VNA to measure parameters like S11 and S21 against manufacturer datasheets. Once baseline functionality was certified, the next step was incremental integration by connecting complementary components. After successfully verifying each segment, components were sequentially added in the chain until the entire TX and RX lines were combined, culminating in a full system performance verification of successful transmission and reception through GNU Radio.

4. Devices used for testing

4.1 Vector Network Analyzer

The device used to extract the scattering parameters (S-parameters) of the RF modules is the Chelegance JNCRadio VNA 3G vector network analyzer (VNA). It is a portable two-port instrument equipped with SMA connectors, capable of analyzing the frequency band between 50 kHz and 3 GHZ with a dynamic range of up to 70 dB for the S21 parameter and 50 dB for S11 [13]. Since both DUTs operate at frequencies starting from 2 GHz, the analysis focused on the useful overlapping window (2–3 GHz). Prior to data acquisition, the reference plane was aligned to the terminals of the DUT by performing a standard SOLT (Short, Open, Load, Thru).

4.1.1 Scattering Parameters

The testing campaign performed with the VNA regarded mainly the characterization of the device's scattering parameters. Scattering parameters (S-parameters) describe the electrical behavior of linear radio frequency (RF) and microwave networks in response to incident wave signals. The most indicative, as covered in [15,16], are:

- S11 (Input Reflection Coefficient) : The ratio of power reflected back from the input port to the power incident upon it. It evaluates how well the amplifier's input impedance is matched to the system, directly correlating to the Voltage Standing Wave Ratio (VSWR)
- S21 (Forward Transmission Coefficient): The ratio of power exiting the output port to the power entering the input port. For an amplifier, this measurement represents the device's forward gain

Copyright ©2026 by the International Astronautical Federation (IAF). All rights reserved.

4.1.2 Attenuators used

To prevent distortion and maintain operation within the linear, small-signal regime, both amplifiers required power management at the input. The PE15A1010 has a 1 dB compression point (P1dB) of 14 dBm [6], while the PE15A4011 is a high-power module with a P1dB of approximately 36.5 dBm [8]. Directly applying the VNA's stimulus power (up to -9 dBm) would yield theoretical outputs of +31 dBm for the PE15A1010 [6] and +23 dBm for the PE15A4011. To keep the PE15A1010 strictly out of saturation, and to prevent the PE15A4011's +23 dBm output from overloading the VNA's receiving port, a calibrated attenuator was inserted between Port 1 of the VNA and the RF-IN port of each amplifier during their respective tests.

4.2 Spectrum Analyzer

To evaluate the radio frequency transmissions generated by the software-defined radio setup-utilizing Nuand bladeRF boards equipped with BT-100 and BT-200 Bias-Tee modules for inline component power injection spectral analysis was performed using a tinySA Ultra+ ZS407 [17]. This portable spectrum was operated in Ultra mode that extends level-calibrated observation up to 7.3 GHz [17]. The device is equipped with switchable resolution bandpass filters, an optional 20 dB built-in LNA, and an input step attenuator ranging from 0 dB to 31 dB [17]. To safeguard the instrument against exceeding its maximum input threshold of +10 dBm, direct coaxial connections were avoided. Instead, the tinySA was utilized to safely capture and measure the SDRs' output signals over the air via an attached antenna.

5. The testing campaign

5.1 PE15A1010

To successfully characterize the PE15A1010 primary LNA, the device was powered directly from a 12 V DC power supply. Port 1 of the NanoVNA was connected to the amplifier's RF IN and Port 2 to the RF OUT. This specific RX pipeline test was performed without the secondary BT-200 LNA in the chain. This omission was due to the absence of a standalone bias-tee injector [7] required to power the BT-200 on the test bench; however, the BT-200's functionality has been verified in other C3 applications[2][3] and is powered directly by the SDR's internal bias-tee in the final integrated ground station. Because the PE15A1010 acts as a high-gain amplifier, a crucial hardware precaution during this setup was placing a physical inline RF attenuator. Without this attenuator, the massive RF amplification would have saturated or permanently damaged the VNA's internal receivers [13].

5.1.1 VNA: S11 and S21 parameters

As shown in Fig.3, the amplifier's forward gain aligns perfectly with the datasheet specifications [6]. At the 2.0 GHz marker, an S21 measurement of 39.92 dB was recorded. Across the entire 2.0 GHz to 3.0 GHz sweep, the gain remains remarkably flat and consistent. This validates the manufacturer's claim of 40 dB typical gain [6] and guarantees that the amplifier will provide the stable amplification necessary to overcome the subsequent coaxial cable insertion losses in the receiving chain without distorting the signal.

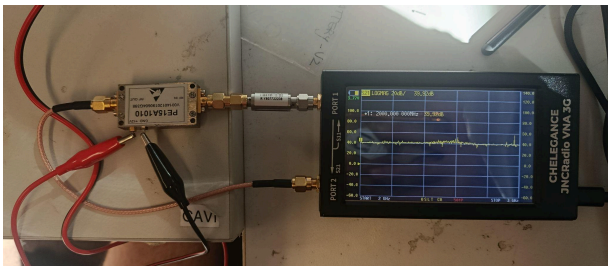

Fig. 3 S21 PE15A1010

As important as the raw amplification is the LNA's ability to absorb faint signals without reflecting them back toward the antenna. In Fig. 4, the measurement captures the input return loss, with the marker at 2.5 GHz reading -23.54 dB. Throughout the entire S-band sweep, the S11 trace consistently fluctuates well below the -10 dB threshold, averaging around -20 dB. This deep return loss ensures maximum power transfer from the diplexer into the LNA, minimizing standing waves.

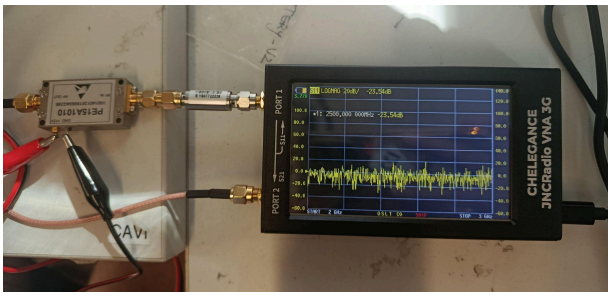

Fig. 4 S11 PE15A1010

5.1.2 SA: Estimation of the noise factor

To try estimating LNA's NF the method proposed is the Cold Source. Unlike the standard Y-factor method [18], which requires a calibrated active noise source, this approach relies on the fundamental Johnson-Nyquist thermal noise generated by a passive 50-ohm termination at room temperature, which provides a known baseline noise power density of -174 dBm/Hz [5].

The amplifier's insertion gain G was first measured with the NanoVNA, then a 50-ohm termination was

Copyright ©2026 by the International Astronautical Federation (IAF). All rights reserved.

connected directly to the RF input of the TinySA to measure and store the instrument's intrinsic noise floor [17].
The 50-ohm termination was moved to the LNA input to act as the thermal noise generator. The LNA output was connected to the analyzer, and the total amplified noise power $P_{measured}$ was recorded.

The formula used for the NF estimation, following [5], was:

$$NF = P_{measured} + 174 - G - 10 * log_{10}(RBW)$$

The SA had an internal function that could calculate it automatically after tuning it just by inserting the G, that was calculated in point 5.1.1 (S21) [17] .

The calculation resulted in a negative Noise Figure, a physical impossibility implying that the amplifier reduced the ambient thermal noise. This mathematical artifact highlights the fundamental limitations of the Cold Source method [18] when executed with low-cost or low-dynamic-range instrumentation. The failure of the test was reconducted to these two possibilities:

- Instrument Noise Masking: The intrinsic noise figure of the spectrum analyzer was significantly higher than that of the LNA. Despite mathematical compensation, the instrument's internal noise completely masked the extremely low noise output of the DUT.
- Extreme Sensitivity to Gain Uncertainty: The Cold Source algorithm subtracts the externally measured gain from the total noise power. Because the method provides no built-in self-correction, even a fractional overestimation of the LNA's gain during the VNA stage propagates directly into the formula, easily driving the final NF value below zero.

5.2 PE15A4011

To characterize the PE15A4011 the same NanoVNA setup was utilised (Fig. 5), again employing a 50 dB attenuator on the VNA's receiving port to protect the sensitive internal receivers from the HPA's massive output power. However, a significant hardware constraint was encountered during this specific test regarding the DC biasing. The HPA requires an 8 V drain voltage (Vds) and draws substantial current to reach its full RF output [8]. During the initial bench setup, the high current demand triggered the overcurrent protection mode on the laboratory power supply. To safely proceed with the RF characterization without crashing the power supply, the amplifier was deliberately under-drove by supplying a reduced drain voltage of 5 V.

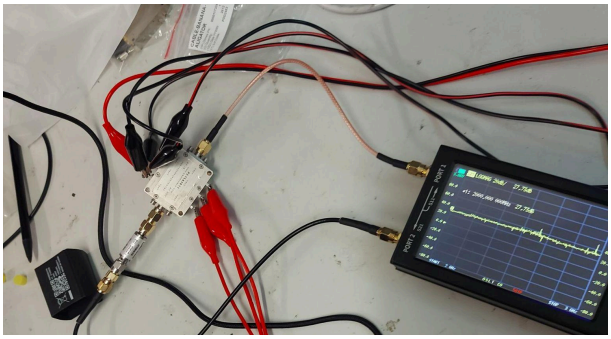

Fig.5 PE15A4011 testing setup

5.2.1 VNA: S11 and S21 parameters

The impact of this reduced voltage is directly reflected in the forward gain measurements. As shown in Fig. 6, S21 was recorded at the 2.0 GHz marker to be 27.69 dB. While this is lower than the typical 32 dB specified in the datasheet [8], this discrepancy is entirely expected due to the 5 V power restriction throttling the amplifier's maximum potential. Despite operating in an under-powered state, the S21 trace remains stable and relatively flat across the entire 2.0 GHz to 3.0 GHz sweep, to confirm that the amplifier is functioning correctly and linearly within the S-band [19,20].

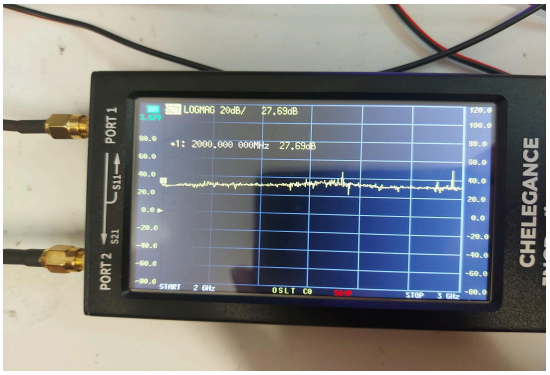

Fig.6 S11 PE15A4011

The measurement displayed in Fig.7 validates the amplifier's input impedance matching: at the 2.0 GHz marker, the input return loss reads -10.72 dB, and the trace continues to fluctuate around or below this standard -10 dB threshold across the active frequency band. This is an acceptable 50-ohm impedance match at the RF input, even under non-ideal DC biasing conditions. This proper matching ensures that the pre-amplified signal coming from the BT-100 driver stage will smoothly transfer into the HPA without generating severe standing waves or reflecting power back down the transmission line.

Copyright ©2026 by the International Astronautical Federation (IAF). All rights reserved.

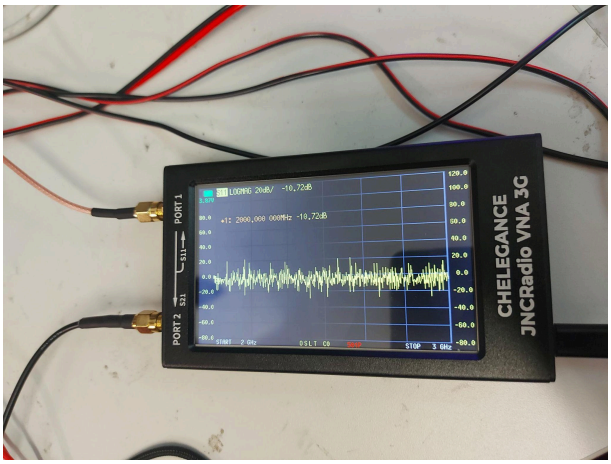

Fig.7 S21 PE15A4011

5.3 Diplexer JFCD1400T2400SF

The verification of the diplexer focused on validating its scattering parameters and port-to-port isolation to ensure strict separation between the transmission and receiving channels. Because the diplexer is a 3-port device and the testing utilized a 2-port NanoVNA, the procedure required terminating the unused port with a perfectly matched 50-ohm load, as shown in Fig. 8. This allowed accurate 2-port measurements while simplifying the procedure. Prior to measuring, a full Open-Short-Load-Through calibration was performed.

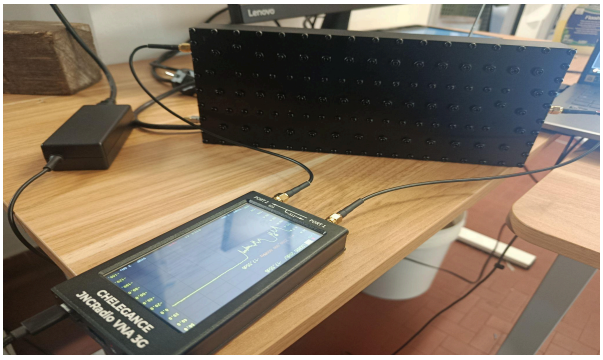

Fig. 8 Diplexer VNA test

The key performance requirements, stated in the documentation [19] are:

-Operating Frequencies: The device must cleanly separate the TX/Uplink range (2025–2120 MHz) from the RX/Downlink range (2200–2400 MHz).

-Return Loss (S11): Must remain lower than -10 dB across both operational frequency ranges to guarantee proper impedance matching.

-Insertion Loss: The forward transmission loss within the active passbands must be less than 1 dB to minimize signal degradation.

-Port-to-Port Isolation: The diplexer must provide at least 50 dB of isolation (e.g., cross-port transmission < -50 dB) in the rejected frequency bands, which is essential to protect the receiving LNA from the high-power transmission signal.

To extract this data, the testing campaign involved performing a full S-parameter measurement sweep from 2.0 GHz to 3.0 GHz, utilizing a VNA test power of 0 dBm.

5.3.1 VNA: S-parameters

-Transmission Channel (CH2 / Uplink: 2025–2120 MHz): As demonstrated in Fig. 9 and Fig.10 , the uplink passband exhibits an insertion loss (S21) comfortably below the 1.0 dB requirement, hovering near 0 dB across 2.025–2.120 GHz. The in-band return loss (S11) remains consistently below -18 dB (reaching notches down to -45 dB), satisfying the requirement of S_11 < -10 dB. Beyond 2.200 GHz, transmission drops sharply into the instrument noise floor at -65 dB to -80 dB, exceeding the 50 dB isolation threshold.

-Reception Channel (CH1 / Downlink: 2200–2400 MHz): As shown in Fig. 11 and Fig. 12, the downlink channel maintains near-zero insertion loss S21 > -0.5dB across the full 200 MHz passband (2.200–2.400 GHz). Out-of-band rejection in the uplink segment (2025–2120 MHz) reaches between -60 dB and -90 dB, ensuring strong port-to-port isolation to protect the PE15A1010 LNA from the high-power transmit signal. The parameter S11 stays between -15 dB and -40 dB throughout the operational band.

-Common Port Impedance Matching: In both dual-trace captures, the common antenna port return loss (S11) demonstrates sharp, well-defined resonance notches (< -15dB) exclusively within the two operational windows (2025–2120 MHz and 2200–2400 MHz). In the transitional guard band (2120–2200 MHz) and beyond 2.400 GHz, S11 approaches 0 dB, confirming total out-of-band energy reflection.

Copyright ©2026 by the International Astronautical Federation (IAF). All rights reserved.

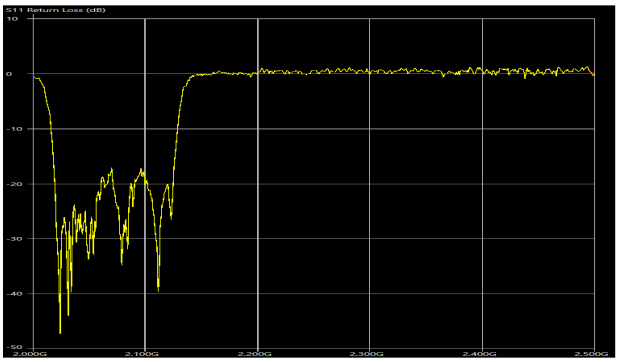

Fig. 9 S11 CH2to CH1

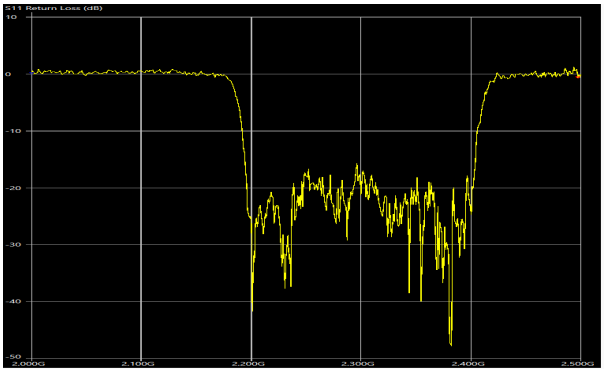

Fig. 10 S11 CH1 to CH2

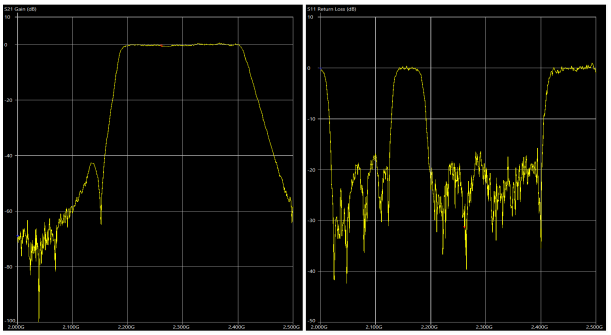

Fig. 11 S21 and S11 IN to CH1

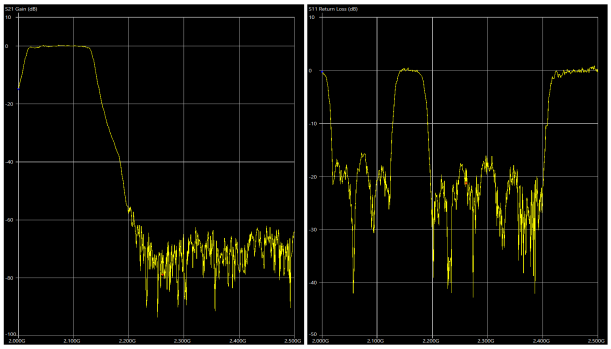

Fig. 12 S21 and S22 IN to CH2

6. DSP and GNU Radio

The decision to use GNU Radio to manage the signals generated and received by the ground station was driven by the software's versatility and open-source ecosystem. At the core of the digital processing pipeline is a Nuand bladeRF 2.0 micro Software-Defined Radio, configured with the hostedxA9.rbf FPGA firmware to maximize its on-board processing capabilities [20]. To connect this physical SDR hardware with the digital signal processing flowgraphs, the Osmocom framework was utilised: specifically, the gr-osmosdr source and sink blocks were used in GNU radio to exert precise control over the bladeRF's radio emissions and reception parameters [12].

6.1 The SDR: Nuand BladeRF XA9

The core of the RF pipeline is the Nuand bladeRF 2.0 micro xA9 that fills the gap between analog radio hardware and digital GNU Radio flowgraphs.This specific Software-Defined Radio was selected primarily for its extensive frequency range, which spans from 47 MHz all the way to 6 GHz, effortlessly covering S-band requirements and VHF/UHF [3]. It is also capable of handling up to 61.44 MHz of bandwidth and features a 2x2 MIMO architecture that provides more than enough capacity to process wideband, high-data-rate downlink [20].

Especially for this specific hardware architecture, the bladeRF includes software-switchable bias-tees on its SMA RF ports. This built-in capability allows powering up the BT-100 driver and the BT-200 directly over the coaxial cables, simplifying control room's setup and reducing the complexity of the DC power distribution.

6.2 BPSK modulation

To transmit data effectively, Phase Shift Keying (PSK) was used, a digital modulation process that conveys data by altering the phase of a constant-frequency carrier wave. This scheme operates by mapping specific bit patterns to a finite number of allowed phases. At the receiving end, a matched demodulator evaluates the phase of the incoming signal and maps it back to its corresponding symbol to recover the original data. For this S-band implementation, Binary Phase Shift Keying (BPSK) was specifically chosen , which is a robust form of PSK. BPSK utilizes just two distinct phases separated by exactly 180° to represent binary 1s and 0s. BPSK was selected as a baseline modulation scheme for the initial testing campaign because of its simple constellation and well-established error-performance characteristics [21,22]. The achievable error rate depends on the available E_b/N_0, which must be assessed through a mission-specific link budget accounting for

Copyright ©2026 by the International Astronautical Federation (IAF). All rights reserved.

propagation losses, antenna gains and pointing losses, receiver noise, and data rate [9].

6.3 TRX code and testing

After testing and validating each device, the next step is the testing campaign that is TRX testing, together with the amplifiers and the SDRs.

A test environment was set to evaluate the flowgraph, but the diplexer wasn't used as the goal was to simulate a "real-case scenario" of communication between two devices in short distance. One Computer was the transmitter, with its TX code, TX pipeline and SDR, and a PC was the receiver, with its RX code, RX pipeline and SDR.

The code that was used for this first test was built starting from the GNU Radio codes implemented in the other two bands, changing frequency (the 2255 MHz was selected as the central frequency) and some details about Gain, data rate and modulation.

The antennas used were short 6.7 cm monopole antennas adapted for the working frequency.

Given the short distances between RX and TX antennas, due to limited test environment space, for the tests a 50 dB attenuator was used to prevent any damage to the devices and the people involved, that lead to lower gains detected by the radio software, that were considered in the tests' conclusions.

6.3.1 RX pipeline and results

The first code and setup that was tested was the RX one, which obviously didn't catch any signal because of no source, but was at least used to see if the code worked (Fig. 13) and there weren't any problems with the PC-SDR interface. The RX pipeline consisted in:

PC ← SDR ← BT-200 LNA ← PE15A1010 ← 50 dB attenuator ← Antenna

As shown in Fig. 14 .

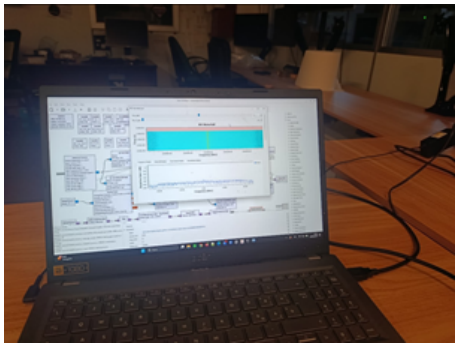

Fig.13 Working code for RX and GUI



Fig. 14 RX pipeline setup

6.3.2 TX pipeline and results

On another computer, the code for transmission was tested. The spectrum of the transmitted signal in BPSK modulation is shown in Fig. 15. The waterfall spectrogram confirms the stability of the transmission. The continuous power distribution across the active channel demonstrates stable signal generation without transient dropouts or unwanted spectral drift over time. Below this, the central Fast Fourier Transform (FFT) plot characterizes the signal in the frequency domain. The spectral footprint exhibits a defined main lobe that delineates the primary occupied bandwidth, characterized by the symmetrical sidelobes characteristic of a BPSK signal. The constellation diagram at the bottom validates the mathematical accuracy of the digital modulation. The symbols are tightly clustered into two distinct states strictly along the horizontal In-Phase (I) axis, maintaining a zero-amplitude component in the Quadrature (Q) domain. This visually confirms the 180° phase separation in the BPSK modulation.

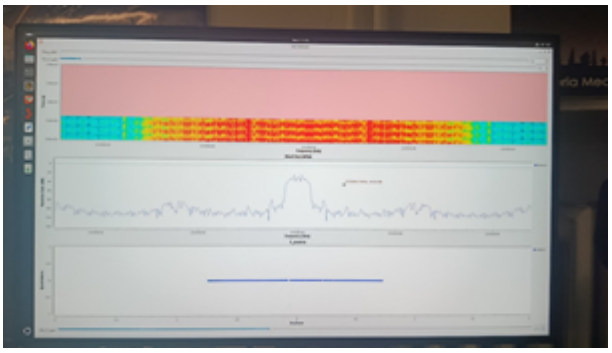

Fig.15 TX GUI

The TX pipeline is similar to the RX one:

PC → SDR → BT-100 → PE15A4011 → 50 dB attenuator → Antenna

As displayed in Fig. 16.

Copyright ©2026 by the International Astronautical Federation (IAF). All rights reserved.



Fig. 16 TX pipeline setup

The transmitting power signal through the SA was sensed as a spike, as seen in Fig 17. Also the WIFI spectral occupation at 2.4 GHz was detected.

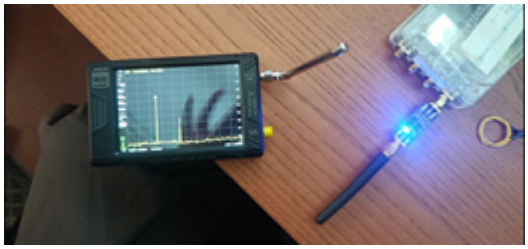

Fig. 17 TX Power and WIFI spectral occupation

6.3.3 TRX pipeline and results

For the final TRX testing, only the BT-100 was used for the amplifiers in the TX pipeline, while the BT-200 was dedicated to the RX line (as shown in Fig. 18). This configuration eliminated the need for external attenuators, allowing for the direct observation of transmission and successful signal reception in the RX spectral diagram .

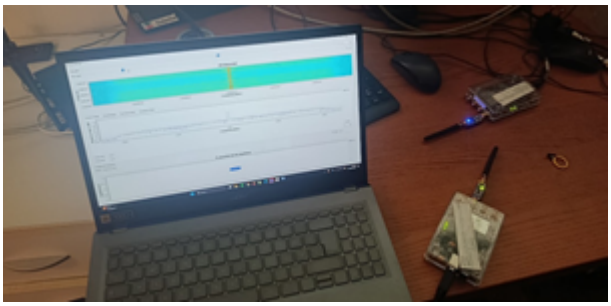

Fig. 18 TRX testing setup

In Fig. 19 it is shown the raw baseband signal exactly as it is received and processed by the GNU Radio flowgraph.
The upper waterfall confirms a successful reception: a sharp, distinct spectral peak above the noise floor.
There is however a problem with the constellation diagram at the bottom of the interface. Instead of the two discrete phase states expected, the plot displays a circular ring that indicates continuous phase rotation over time, which is a classic behavior of a carrier frequency offset.
So the physical layer is capturing the analog signal, but to extract the message from this rotating signal, the final GNU Radio receiver flowgraph must incorporate carrier synchronization blocks such as a Costas loop to track the phase error, arrest the rotation, and collapse the ring back into the correct binary symbols for demodulation.

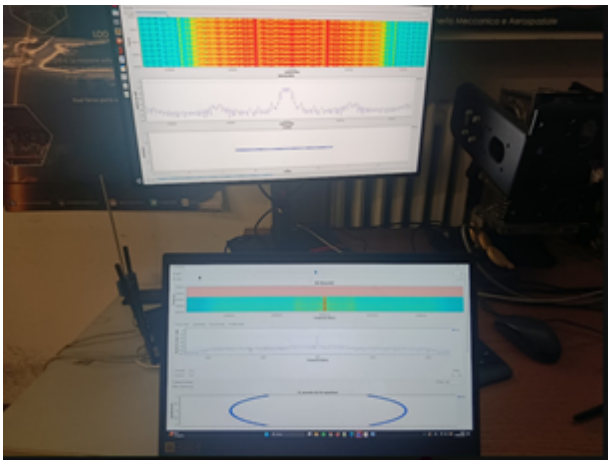

Fig. 19 TRX test results

6.4 New code under development in closed loop

After working on the previous Gnu Radio code, a new pipeline was developed using the resampling parameters and flowgraph reported in [6, Fig. 11]. This new iteration is following the same principle of the previous one, with a simpler packet framing and deframing, using gnuradio modules, rather than more complex custom python code block. Furthermore a working CRC32 check was added. The complete flowgraph can be seen in Fig.20.

After developing the described new code, once again it was tested, following a slightly different approach: before testing with antennas and two different devices for rx and tx, a software test environment was set up, so the complete signal-processing pipeline was tested. The transmit and receive processing chains were connected through a virtual link using Virtual Sink and Virtual Source blocks. This configuration was used to check the processing logic and the modulation and demodulation stages before introducing the SDR hardware and RF components.

Finally, a proper test was conducted in the same environment described in point 6.3, this time we've been able to properly have a working communication link between two different devices, one transmitting a long text excerpt from Dante's *Divina Commedia* and

Copyright ©2026 by the International Astronautical Federation (IAF). All rights reserved.

another one receiving it. A longer text excerpt was selected because missing, corrupted, or discarded portions would be more apparent in the reconstructed output, comparing it with the input.

7. Application of the S-band to the ELECTRA mission

The S-band communication chain developed and tested in this work is preparatory for the operations of ELECTRA, the upcoming mission of CubeSat Team PoliTo.

7.1 ELECTRA mission overview

ELECTRA is a 3U CubeSat mission designed to map the ionospheric Total Electron Content (TEC) using dual-frequency GNSS receivers, and to demonstrate a solid-state micro thruster through GNSS-based Precise Orbit Determination (POD).

Both objectives rely on collecting GNSS payload data from two separate GNSS receivers at variable sampling rates (1Hz - 10Hz). While previous CubeSat Team PoliTO missions [1] used sub-GHz amateur bands, the transmission of the produced data cannot rely on an amateur UHF link alone. Data budget simulations and science operations requirements, taking into account the expected payload data generation and the visibility time during passes, suggest that a 512 kbps downlink data rate is the minimum viable option, with 2048 kbps being the preferred option for long periods of continuous GNSS data collection.
For this reason, a S-band link acts as the primary channel for payload data transmission and is used for telecommands, while a separate UHF link is intended to be used for amateur radio operations such as digipeater service and beacon transmission, fostering collaboration with the amateur radio community. The UHF link also guarantees basic telemetry and telecommand in case of loss of attitude control or other subsystem failures.

This operational need is the motivation for extending C3 with multi-band capabilities, and the presented testing campaign is a step towards support for ELECTRA's mission needs.

7.2 Compatibility between C3 and ELECTRA

The onboard S-band transceiver currently baselined for ELECTRA is the Satlab SRS-4 (upgraded from the Satlab SRS-3 which was assumed in previous ELECTRA iterations [4]), which transmits in the 2200–2290 MHz range and receives in the 2025–2110 MHz range, supporting BPSK, QPSK and 8PSK modulations at symbol rates between 100 and 5000 kBd. The RF components characterized and integrated in this work have been selected and tested to operate in this frequency range. This is a preliminary indication of hardware compatibility between the space and ground segments.

While the spacecraft RF hardware still has to undergo procurement, the testing campaign of C3 serves as a preliminary validation of link compatibility between the ground and space segments. The BPSK modulation tested in GNU Radio covers the most likely in-orbit modulation configuration.

7.3 Ground segment role in ELECTRA science operations

The POD and TEC post-processing is carried out on ground, and it is therefore necessary to downlink raw GNSS data. A reliable S-band link is crucial for maximizing the science data sent to ground at each pass and, as a consequence, scientific return.

In the latest iteration of the Link and Data Budget Analysis performed for ELECTRA, a 40dB LNA gain was assumed, corresponding to the parameter characterised for the LNA in this work. The RF campaign therefore provides confirmation of the assumptions made for the link budget analysis, strengthening confidence in the feasibility of payload data transmission under the required data rates with the current configuration.

7.4 Future perspective

If validated during in-orbit ELECTRA operations, C3 would be consolidated as a high-datarate multi-band ground station, supporting future student-led space projects at Politecnico di Torino with comparable or higher data requirements.

8. Next steps: Final integration in the pre-existing structure

8.1 HW integration

Following the successful completion of the standalone bench testing, the final milestone is the physical integration of the S-band hardware into the pre-existing structure of the C3 GS. To ensure long-term reliability and operational safety, the entire assembly procedure strictly adheres to AIVT protocols, following the internal integration guidelines [3,14].

The physical hardware layout directly mirrors the architectural pipeline illustrated in Fig. 3. For the RF signal paths, low-loss LMR-200 coaxial cables terminated with standard SMA connectors were utilised. During the physical assembly, extreme care is taken to route these RF lines efficiently, minimizing cable

Copyright ©2026 by the International Astronautical Federation (IAF). All rights reserved.

lengths to prevent unnecessary insertion loss that could degrade the link budget. Furthermore, all SMA connectors must be tightened to the correct specification using a calibrated torque wrench; this ensures optimal 50-ohm impedance matching and prevents signal reflections or mechanical loosening over time.

Equally critical to the RF routing is the DC power distribution network. The primary power source driving the S-band front-end is a KUHNE PSU RSP-320-12, a highly stable industrial power supply capable of delivering a robust 320 W at 12 V DC [24]. Wiring this power supply requires strict procedural compliance to protect the sensitive active components [24]. The DC power cables must be carefully routed away from the unamplified RF lines to prevent induced EMI from coupling into the receiving chain.

When terminating the power connections, all components must share a common, secure ground tied to the station's main chassis.

8.2 SW integration: current status and remaining work

Integration of the S-band functionality into the C3 web application has been implemented at the software level. Users can select the S-band and the desired operating mode (RX or TX), then start the corresponding GNU Radio application through the “Communicate” button. The web server launches the application as a subprocess, providing access to its graphical interface.

The current configuration operates with binary files in place of the physical radio interfaces. In RX mode, the application processes a prepared binary file containing an encoded test signal instead of samples acquired through the SDR. In TX mode, the generated signal is written to a binary file instead of being transmitted through the SDR and antenna.

The remaining integration work concerns communication with the Raspberry Pi for control of the transmit and receive RF-chain power supplies, connection to the SDR hardware, and verification of coordinated operation between the selected software mode and the corresponding hardware configuration.

9. Results and Discussion

The tests summarized in sections 5 and 6 confirm that the S-band line is functional and ready to be integrated in the existing ground segment.

At component level, the performance of PE15A1010 LNA was found to match its datasheet specification almost exactly with 39.92 dB of gain against a nominal 40dB. The PE15A4011 HPA underperformed with a gain of 27.69 dB against a nominal 32dB, but this difference was attributed to the intentional under-driving of the component. The JFCD1400T2400SF diplexer satisfied requirements on operating frequency, insertion loss, return loss and port-to-port isolation.

The noise figure estimation resulted in a non-usable result, giving a negative noise factor. This was attributed to limitations of the Cold Source method when using low-cost instrumentation.

At a system level, the TX and RX GNU Radio pipelines were validated. The TX chain produced a clean BPSK signal with the expected constellation, while in the combined TRX test the constellation showed phase rotation, indicating a carrier frequency offset. This issue was solved at DSP level with a Costas loop. The flowgraph was completed with packet framing/deframing and CRC32. The test was completed with the transmission and reception of a long text.

10. Conclusions

The presented testing campaign successfully characterised the S-band line of C3, both at a component and at a system level. The results also provided a preliminary confirmation of the link budget assumptions for ELECTRA, the upcoming mission of CubeSat Team PoliTo.

Although some issues were encountered throughout the campaign, they were successfully identified and isolated. This is a validation of the “divide and conquer” approach adopted for this project.

The test campaign also successfully fulfilled its formative objective: team members from different engineering fields worked on a hands-on project giving them experience in RF design, measurement techniques, systems engineering and AIVT techniques.

Acknowledgements

The authors would like to thank the members of the CubeSat Team PoliTO, the Department of Mechanical and Aerospace Engineering (DIMEAS) and the STARlab research group for their support during the test campaign. The authors also wish to acknowledge ESA for their support in the development of ELECTRA during the Fly Your Satellite! Design Booster 2 programme.

Copyright ©2026 by the International Astronautical Federation (IAF). All rights reserved.

References

[1] CubeSat Team Polito https://www.cubesatpolito.it, (Accessed 11.09.2026)

[2] S. Campioli, G. Abbate, S. Corpino, F. Stesina, F. Coppa, D. A. Cazacu, V. Frangipani, L. Di Nardo, A. Tomatis, and D. Demoro, "Integration and Testing Campaign of an Educational Satellite Ground Station," in *Proceedings of the 75th International Astronautical Congress (IAC 2024)*, Milan, Italy, Oct. 2024, paper IAC-24/B2/IPB/83257, pp. 1029–1038.

[3] ASSEMBLY, INTEGRATION AND VERIFICATION (AIV) PLAN DIMEAS/CST/2020/036/C3/TN/C3_AIV/I2R0 (Technical Note - Internal use document)

[4] S. Campioli et al., An Educational 3U CubeSat Mission at Politecnico di Torino: The ELECTRA Mission for TEC Research and Micro Thruster In-Orbit Testing, IAC-25,E2,4,2,x99834, 76th International Astronautical Congress, Sydney, Australia, 2025, 29 September – 3 October.

[5] Keysight Technologies, "Fundamentals of RF and Microwave Noise Figure Measurements," Application Note 57-1, 2014.

[6] Pasternack PE15A1010: Pasternack Enterprises, 2 GHz to 6 GHz, Low Noise High Gain Amplifier, 40 dB Gain, 14 dBm P1dB, 0.9 dB NF, SMA https://www.pasternack.com/images/ProductPDF/PE15A1010.pdf (accessed 13/09/2026)

[7]Nuand LLC, BT-200 Wideband Receive Amplifier https://www.nuand.com/product/bt-200/, (accessed 13.09.2026)

[8] Pasternack PE15A4011: Pasternack Enterprises, 2 GHz to 4.4 GHz, 5 Watt High Power GaAs Amplifier, 32 dB Gain, 37 dBm IP3, SMA https://www.pasternack.com/images/ProductPDF/PE15A4011.pdf, (accessed 13.09.2026)

[9]Nuand LLC, BT-100 Wideband Transmit Amplifier https://www.nuand.com/product/bt-100/, (accessed 13.09.2026)

[10] JQL Cavity Diplexer: JQL Electronics, S-Band Cavity Diplexer 2025-2120 MHz / 2200-2400 MHz https://www.jqlelectronics.com/wp-content/uploads/2015/08/JFCD1400T2400SF.pdf, (accessed 13.09.2026)

[11] European Cooperation for Space Standardization, *Space engineering-Verification*, ECSS-E-ST-10-02C Rev.1, 1 February 2018. https://ecss.nl/standard/ecss-e-st-10-02c-rev-1-verification-1-february-2018/ (accessed 12/09/2026). European Cooperation for Space Standardization, https://ecss.nl/ (Accessed 5.09.2026)

[12] GNU radio documentation, https://www.gnuradio.org/ (accessed 12.09.2026)

[13] JNCRadio VNA 3G Portable Vector Network Analyzer "Chelegance VNA user manual", rev. 2, https://chelegance.github.io/WIKI/METER/JNCRADIO-VNA-3G/v2_JNCRadio%20VNA%203G%20Portable%20Vector%20Network%20Analyzer%20User%20Manual%20V2.0.pdf (accessed 13/09/2026)

[14] S-BAND LINE INTEGRATION TESTING [TSP]C3-RF-012 (Internal use document)

[15] Keysight Technologies, "Analyzing Data in the Frequency Domain," PLTS documentation, https://helpfiles.keysight.com/csg/N1930xB/Analyzing/Analyzing_Data_in_the_Frequency_Domain.html (accessed 13.09.2026).

[16] Pozar, D. M. (2011). Microwave Engineering (4th ed.). John Wiley & Sons. Chapter 4

[17] tinySA, "tinySA documentation", https://www.tinysa.org/wiki/ (accessed 13.09.2026).

[18] Rohde & Schwarz, "The Y-Factor Technique for Noise Figure Measurements," Application Note 1MA178, 2015.

[19] S-BAND DIPLEXER TEST [TSP]C3-RF-009 (Internal use document)

[20] Valarezo, Darío & Quiñones-Cuenca, Manuel & Mendieta Cabrera, Gabriela. (2020). USER MANUAL: Nuand bladeRF.]BladeRF documentation, https://github.com/Nuand/bladeRF (Accessed 13.09.2026)

[21] D. Staelin, "Communication Systems," Chapter 4, 6.661 Receivers, Antennas, and Signals, MIT OpenCourseWare, Spring 2003. Course details (accessed 11/09/2026)

[22] CCSDS, "Bandwidth-Efficient Modulations-Summary of Definition, Implementation, and Performance," CCSDS 413.0-G-3 (2018), Issue 3,

Copyright ©2026 by the International Astronautical Federation (IAF). All rights reserved.

February 2018, https://ccsds.org/Pubs/413x0g3e1.pdf (accessed 12/09/2026)

[23] N. Saeed et al., "CubeSat Communications: Recent Advances and Future Challenges," arXiv:1908.09501v2, 2020. https://arxiv.org/abs/1908.09501 (accessed 12/09/2026)

[24]Kuhne Electronics Power Supply RSP 320 W 12 https://shop.kuhne-electronic.de/kuhne/de/shop/professionell/prof-zubehoer/prof-schaltnetzgerae/Power+Supply+RSP+320+W+12/?card=1674, (accessed 13.09.2026)

Figures

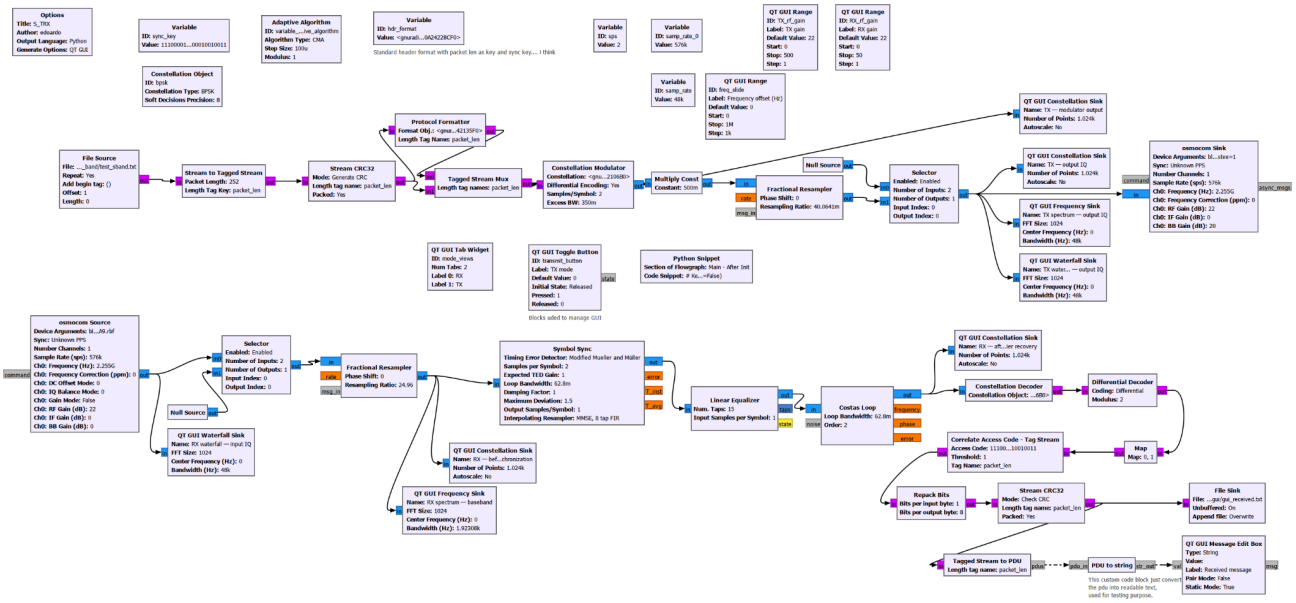

Fig. 20 Gnuradio flowgraph